Mechanical Systems and Signal Processing 80 (2016) 570–581

Contents lists available at ScienceDirect

Mechanical Systems and Signal Processing

journal homepage: www.elsevier.com/locate/ymssp

Misalignment detection in induction motors with flexible coupling by means of estimated torque analysis and MCSA

Carlos Verucchi [a,*], José Bossio [b,c], Guillermo Bossio [b,c], Gerardo Acosta [a,c]

[a] Núcleo INTELYMEC-CIFICEN, Facultad de Ingeniería, Universidad Nacional del Centro de la Provincia de Buenos Aires, Argentina
[b] Grupo GEA Universidad Nacional de Río Cuarto, Argentina
[c] CONICET, Argentina

ARTICLE INFO

Article history:
Received 21 August 2015
Received in revised form
16 March 2016
Accepted 30 April 2016
Available online 6 May 2016

Keywords:
Misalignment
Fault detection
Induction motors

ABSTRACT

In recent years, progress has been made in developing techniques to detect mechanical faults in actuators driven by induction motors. The latest developments show their capability to detect faults from the analysis of the motor electrical variables. The techniques are based on the analysis of the Motor Current Signature Analysis (MCSA) and the Load Torque Signature Analysis (LTSA), among others. Thus, failures such as misalignment between the motor and load, progressive gear teeth wear, and mass imbalances have been successfully detected. In case of misalignment between the motor and load, both angular and radial misalignment, the results presented in literature do not consider the characteristics of the coupling device. In this work, it is studied a mechanism in which the power transmission between the motor and load is performed by means of different types of couplings, mainly those most frequently used in industry. Results show that the conclusions drawn for a particular coupling are not necessarily applicable to others. Finally, this paper presents data of interest for the development of algorithms or expert systems for fault detection and diagnosis.

1. Introduction

Induction motors have become an almost exclusive alternative for developing mechanical power for industrial applications. Given their importance, a major effort has been made in recent decades to develop fault detection techniques. The non-invasive techniques based on monitoring the electrical variables (stator voltage and currents) present the main advantage of their on-line implementation [1–3]. Thus, several techniques have been developed to diagnose stator short circuits, rotor broken bars or end rings, and air gap eccentricity, among others [4].

One possibility to detect and diagnose faults in induction motors consists in analyzing the stator current spectrum (MCSA: Motor current signature analysis) [5,6]. This technique allows the motor diagnosis from sensing the stator currents and therefore its application is fast and economical. A variation of this technique, known as Park's Vector Approach [7], consists in tracking the Vector de Park module. The most important advantages of these techniques are that they are non-invasive and their implementation does not require expensive sensors and data acquisition processes (measurement systems). Load Torque Signature Analysis (LTSA) is an alternative to MCSA [8]. Though this technique requires not only sensing the stator currents but also the applied voltages, the frequency components are more likely to be associated with a

* Corresponding author.
E-mail address: verucchi@fio.unicen.edu.ar (C. Verucchi).

http://dx.doi.org/10.1016/j.ymssp.2016.04.035
0888-3270/

particular fault, which in some cases can be more clearly identified than when using the MCSA.

Progress in the implementation of non-invasive techniques has made it possible to extend the diagnosis of faults to the kinematic chain between the motor and load, even to the load. In [9–11], different techniques for fault detection in gear box driven by induction motors are proposed. In such cases, it is possible to detect gear-teeth wear or breakage from the analysis of the frequency spectrum of the stator currents or the estimated electric torque.

Regarding the driven load, literature presents background on the detection of anomalies from the analysis of electrical variables. For instance, the detection of anomalies in the table of a coal mill is presented in [11]; in [13], the detection of anomalies in an air compressor from the motor variables are shown, and, the detection of cavitation in hydraulic systems with identical strategy is studied in [14].

A study based on the tracking of the stator current and of the active power consumed by the motor to detect misalignment between the motor axes and load is presented in [15]. This paper presents a model that determines the frequencies associated with fault and through experimental tests the feasibility of the proposed method is demonstrated. These tests however are limited to elastic couplings (Rubber Tire-type Couplings) and misalignment on the coupling system may be of great consideration. Results show for example angular misalignment of about 1 to 3 degrees. Though these misalignment angles are within admissible values for elastic couplings, it is important to highlight the capability of the technique for detecting minor misalignments, as they can raise the level of vibration to dangerous levels. A comparison between the MCSA and the vibration analysis can be observed in [16]. This comparison demonstrates that the ability to detect misalignment of MCSA and traditional techniques based on vibration analysis is similar. In addition, [17] also proposes an algorithm able to diagnose faults due to misalignment and mass imbalance for different load conditions. This algorithm compares the fault frequencies of the stator currents with a predetermined admissible value. However, this comparison does not provide criteria to determine failure thresholds. It does not establish differences between different types of couplings either.

This work focuses on misalignment detection. Unlike other works related to the subject, it includes the coupling parameters as variables. In fact, given that there are different choices for power transmission, their comparison is carried out to show the proposed detection technique effectiveness for the most common couplings. Then, it becomes important to establish the criteria to relate the most commonly used fault indicators and angular and radial misalignments.

The theoretical bases that allow to deduce how misalignment events occur on the electric motor torque and the stator current are also presented. Then, experimental results are presented for different types of couplings, and finally conclusions are drawn.

2. Misaligned drives model

It is important to distinguish two types of potential misalignment: angular misalignment and radial misalignment. *Angular misalignment* occurs when there is an angular deviation between the motor shaft and load. This situation is illustrated in Fig. 1a. The degree of misalignment is represented by angle α between the two shafts. When the shafts are perfectly parallel to each other, but not on the same line, *radial misalignment* occurs. This situation can be observed in Fig. 1b. Radial misalignment is more severe as the distance between the two axes of rotation becomes greater. Such distance is indicated as d in Fig. 1b and it will be taken as a reference value to indicate degrees of radial misalignment in experimental tests.

Misalignment situations are very common in industrial applications. They usually arise during the assembly process and can be associated to the motor fasteners, the gearbox or other drive components. They can be also due to the preloads produced in pipes or any other components associated with the load. Misalignment can not only occur as the two types described in Fig. 1 but also as a combination of them.

Mostly elastic couplings are used in these applications. These couplings allow dampening sudden load torque disturbances, avoiding knocks on the wheels of the gearboxes, and reducing vibrations during load transmission. All elastic couplings are able to bear small levels of misalignment. The main purpose of the flexible couplings is to allow misalignment due to the assembly of connected rotors and due to the changes of temperature and operation. In addition, the flexible couplings separate mechanically the rotors so that the rotodynamic design of individual rotors can be carried out separately. However, misalignments of any degree reduce couplings lifetime, increase losses [15], and generate mechanical vibrations and bending stress on axes, which may affect the bearing system severely.

Fig. 2 shows the four different elastic couplings evaluated in this work, mostly used in industrial applications [18]. Jaw Couplings (Fig. 2a) are an inexpensive and easy to mount option for standard power applications. They are able to dampen moderate-impact low-vibration loads. Couplings of this type are not torsionally rigid and can bear some degree of radial and angular misalignment as well as axial movement on the shaft. Gear Couplings (Fig. 2b), on the other hand, show torque high density and are torsionally rigid. They can be either flexible or flexible-rigid couplings. Flexible couplings are able to bear radial and angular misalignment. Metal Ribbon Couplings (Fig. 2c) allow torsion as well as angular and radial misalignment. They require lubrication and have certain limitations of temperature and speed. Finally, Rubber-type Couplings, (Fig. 2d), are able to bear some degree of misalignment at all levels without imposing excessing loads on the bearing system. Their damping properties allow reducing torsion vibrations and oscillations.

As it is shown in [14], misalignment modifies the motor torque according to the following equation:

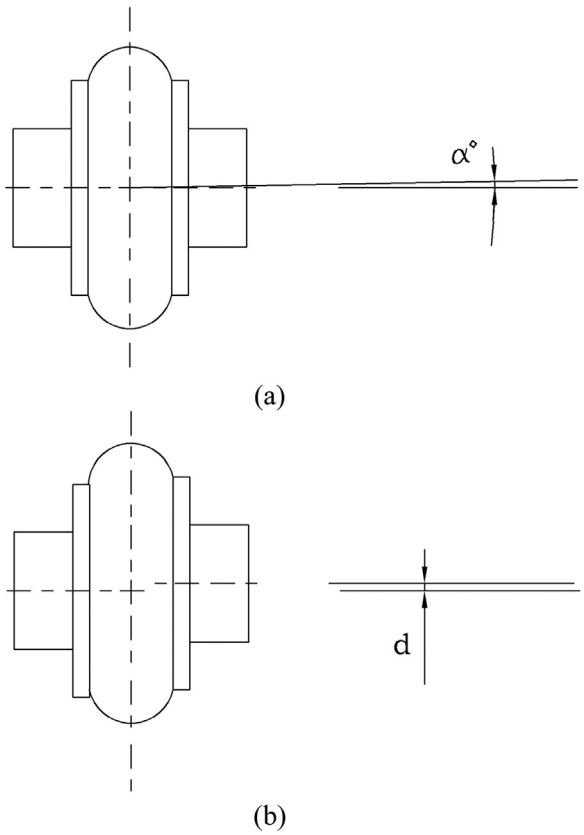

Fig. 1. Angular Misalignment (a), Radial Misalignment (b).

Fig. 2. Different Types of Couplings.

$$T_k = \left[\frac{1}{\cos\ \alpha} - \frac{\sin^2 \alpha}{2\ \cos\ \alpha} - \left(\frac{\sin^2 \alpha}{2\ \cos\ \alpha} \cdot \cos\ 2\theta_l \right) \right] T_l \tag{1}$$

Where α is the misalignment angle (Fig. 1a), θ_l is the angular position of the load with regards to its own rotation axis and T_l is the load torque. Eq. (1) shows that, when α takes a value other than 0, the level of torque the motor must overcome increases progressively its mean value and also incorporates a frequency component $2\theta_l$. This component amplitude increases with misalignment. As for the motor stator current, misalignment occurs through the sidebands around the fundamental component at the frequencies given by:

$$f_s = f \pm n f_r \tag{2}$$

Where f_r is the rotational frequency and n are integers greater than 0. Thus, the fault under study will become evident both on the electrical torque as on the stator current.

This model has been obtained considering a universal coupling between the motor and load, and therefore does not take into account the characteristics due to the coupling nature. Thus, it only provides information about the frequencies associated with failure in both the torque and the stator current.

3. Proposed fault detection method

Two of the most used non-invasive techniques for fault detection in electrical drives are MCSA and LTSA [8]. These techniques consist in analyzing the frequency spectrum of the stator current and torque. Monitoring of the amplitude of the frequency components given by Eqs. (1) and (2) allows monitoring the alignment status of a particular coupling.

Generally, it is not possible to measure directly the torque provided by the motor and therefore, a rough estimation of it is used. Such estimation is carried out from the measurement of the stator voltages and currents according to the following equation [19]:

$$T_e = (3/2)(P/2)(\lambda_{ds} \cdot i_{qs} - \lambda_{qs} \cdot i_{ds}) \tag{3}$$

Where P is the number of poles, and λ and i are flux and current on axes d and q. Flux linkages are obtained as,

$$\lambda_s(t) = \int_0^t \left[v_s(t) - R_s \cdot i_s(t) \right] . dt + \lambda_s(0) \tag{4}$$

Where voltages and currents are denoted as follows:

$$v_s(t) = v_{qs}(t) + j\ v_{ds}(t) \tag{5}$$

$$i_s(t) = i_{qs}(t) + j\ i_{ds}(t) \tag{6}$$

Torque estimation requires besides sensing currents and voltages, knowing the stator resistance and number of poles of the motor.

The structures of the LTSA and MCSA methods are presented in a block diagram in Fig. 3.

4. Experimental results

Some experimental tests are designed to determine the capability to detect misalignment of the proposed techniques when applied on different couplings. For this purpose, a 3 kW, 4 pole, 50 Hz 380 V induction motor, coupled to a DC machine is used. The motor is mounted on a swivel base that allows imposing angular misalignment conditions to the coupling. Radial misalignment is controlled by the horizontal displacement of the motor respect to load. This assembly can be observed in Fig. 4. All the couplings used in these tests were selected depending on the transmitted torque, rotation speed, load and the rotor shaft diameters, as required by commercial catalogs. Data were collected from a 16 bit National Instruments Acquisition Card and Labview™ software at a rate of 10 kSamples per second.

First, a comparison of the diagnosis variables is carried out for alignment and a 1.5 mm radial misalignment. For this comparison, a Jaw Coupling is used. Fig. 5 shows the frequency spectrum of the estimated torque for the case of shaft alignment. These results correspond to 75% of the nominal power. For such load condition, the rotational speed of the motor is 1452 rpm and the rotational frequency is 24.2 Hz is. An additional component of the rotational frequency, (fr), is also observed in Fig. 5.This component may be due to either load mass imbalance or rotor eccentricity. The same figure also shows the absence of components at twice the rotation frequency ($2fr$), which, as it is shown in Section 2, are able to detect fault misalignment. Fig. 6 shows the frequency spectrum for 1.5 mm radial misalignment. In this particular case, it can be clearly observed a component ($2fr$), and another component, ($3fr$) of greater amplitude. These components clearly show misalignment between the motor axis and load. Furthermore, it can be observed that the component fr for misalignment is higher than that for aligned shafts. This increase can be explained by the additional forces due to misalignment on motor shaft extension. Such forces increase the rotor eccentricity which appears a component at fr. From this comparison, it can be

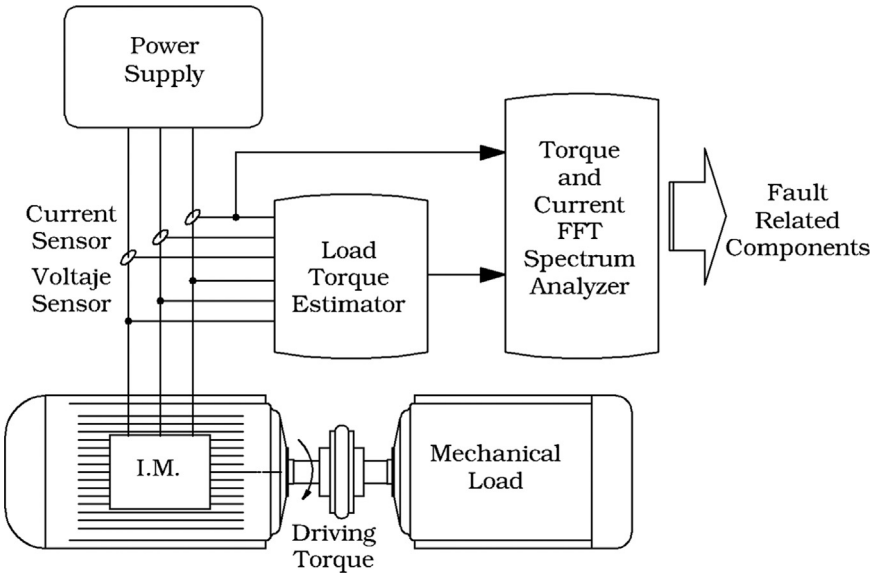

Fig. 3. Functional Block Diagram of the LTSA and MCSA Fault Detection Methods.

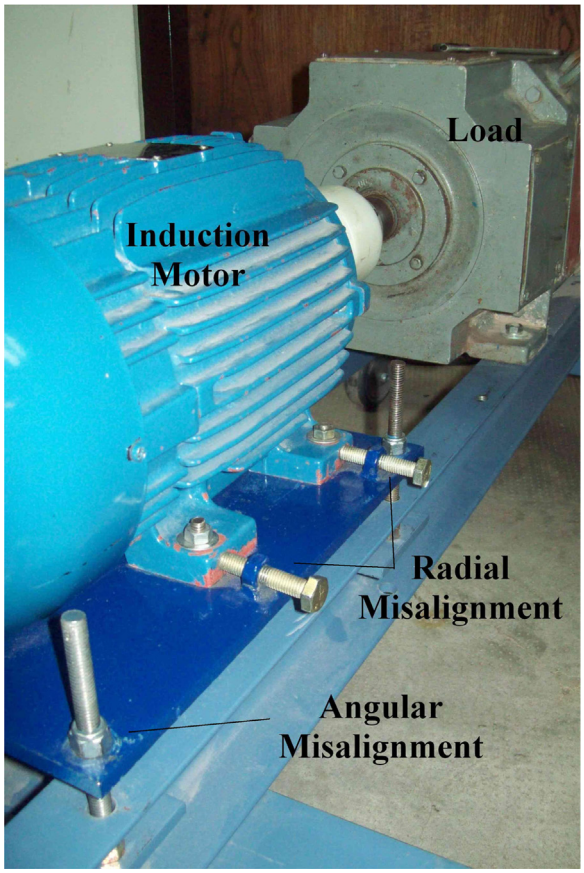

Fig. 4. Laboratory Assembly.

concluded that as for component *2fr* as for *3fr*, they both allow diagnosing faults due to misalignment.

Regarding currents, the fault under study appears at the sidebands shown in Eq. (2). Figs. 7 and 8 show the frequency spectrum of the stator current for the alignment and load conditions shown in Figs. 5 and 6. Fig. 7 shows the sidebands at frequencies $f \pm fr$, associated to the component *fr*, which appear in the motor torque (Fig. 5), whereas it cannot be observed

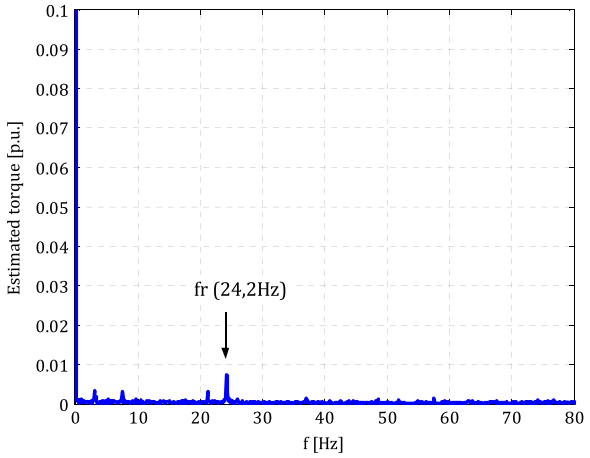

Fig. 5. Estimated Torque Frequency Spectrum, Jaw Coupling, 75% of load, aligned Shafts.

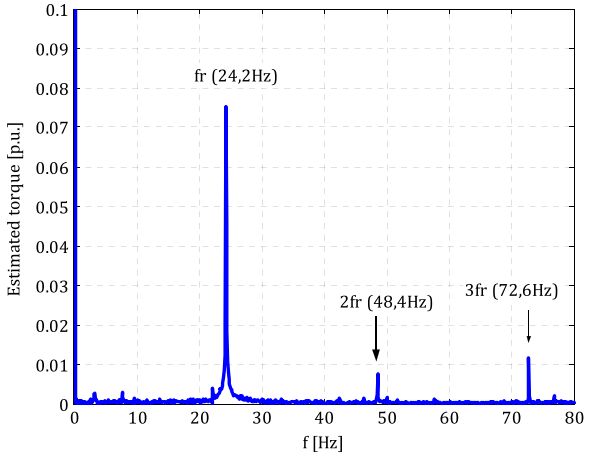

Fig. 6. Estimated Torque Frequency Spectrum, Jaw Coupling, 75% of Load, 1.5 mm, Radial Misalignment.

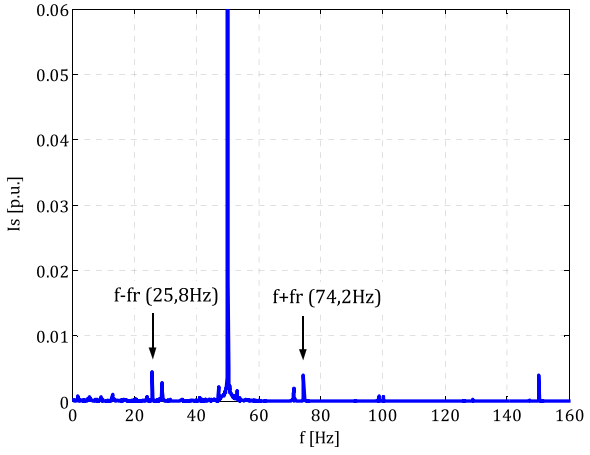

Fig. 7. Stator Current Frequency Spectrum, Jaw Coupling, 75% of Load, Aligned Shafts.

components at $f \pm 2fr$ or $f \pm 3.fr$. Fig. 8 shows misalignment in the coupling expressed by means of components at $f+2fr$ and $f+3fr$.

Then, from this first study, it is possible to check both the analysis of the stator currents and the torque estimation to demonstrate radial misalignment. Similar tests allow to extend these conclusions to angular misalignment cases.

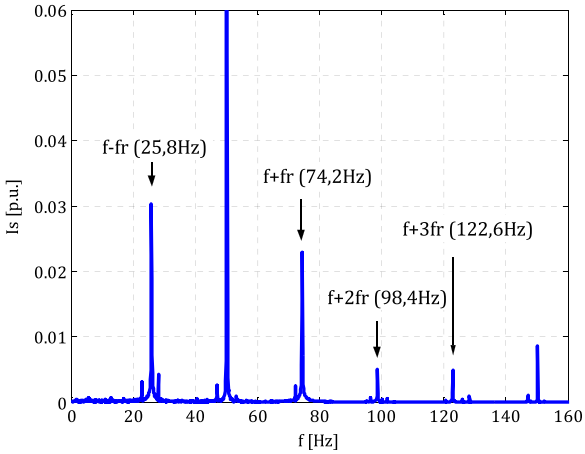

Fig. 8. Stator Current Frequency Spectrum, Jaw Coupling, 75% of Load, 1.5 mm Radial Misalignment.

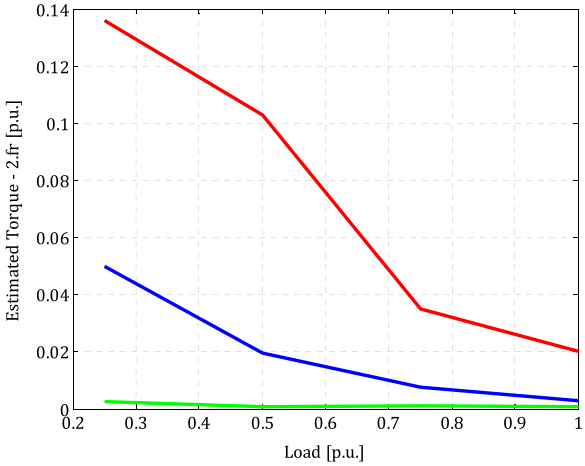

Fig. 9. Components at twice the rotation frequency. Values in p.u. Green: Alignment, Blue: 0.75 mm Radial Misalignment, Red: 1.5 mm. Radial Misalignment. (For interpretation of the references to color in this figure legend, the reader is referred to the web version of this article.)

Results from Figs. 5–8 are obtained with 75% of the nominal load. However, as it can be observed in [16], the amplitude of the components associated to the fault under analysis may vary significantly with the motor load. With the objective of evaluating the motor behavior for different load levels, several tests were carried out for different degrees of misalignment and for variable load values ranged between 25 and 100% of the nominal power. All the tests were performed with different coupling, starting with the same alignment condition and then varying radial and angular misalignment. The remaining variables for the experiments were kept unchanged. Figs. 9 and 10 show the amplitude of the component at $2f_r$, expressed in Nm and p.u., respect to the mean torque, respectively. These figures allow comparing the obtained components for alignment and for two different levels of radial misalignment, both in a Jaw Coupling. It can be deduced from the curves in the same figures that the fault indicators, expressed in both Nm. and p.u., show a tendency to decrease as the motor load increases. Moreover, it can be clearly observed that this relationship between indicators and load is nonlinear. Also, these fault indicators increase with the fault severity (0.75 mm and 1.5 mm misalignments, respectively).

Figs. 11 and 12 show the results for radial misalignment at the component at $3f_r$. Conclusions are similar to those for the component at $2f_r$. The values of the component at *3fr* show a strong dependence on load, to such an extent that for certain load levels, the most severe fault appears less noticeable than the least one. This observation allows concluding that the indicator that best suits misalignment is the component at $2f_r$.

Figs. 13 and 14 present results for angular misalignment. Misalignment levels are ranged from 0.5° to 1°.The Jaw Coupling used for this test is the same used in previous tests. Conclusions are similar to those obtained for radial misalignment, i.e., a decrease in the fault indicator, in p.u. and Nm, with a decrease in load and erratic variation of the component *3fr*.

It is important to notice that the misalignment levels used for the comparison, as for radial as for angular misalignment, are low as the couplings under study are also able to bear high misalignment degrees.

The results obtained using a Jaw Coupling presented in Figs. 9–14 allow validating the conclusions drawn in [15,16]. The only difference is that it considers lower levels of misalignment to demonstrate the capability to detect incipient faults. The

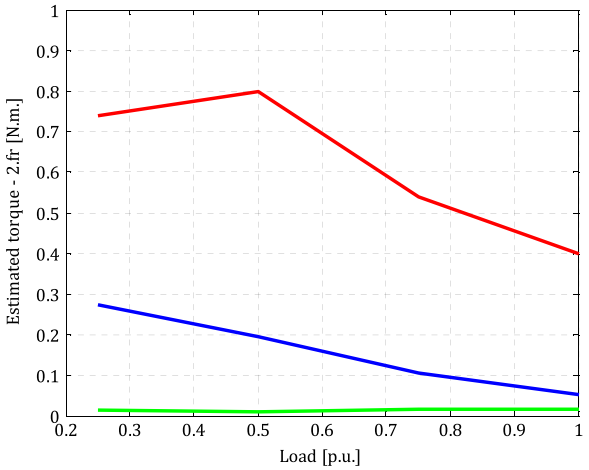

Fig. 10. Components at twice the rotation frequency. Values in N.m. Green: Alignment, Blue: 0.75 mm Radial Misalignment, Red: 1.5 mm. Radial Misalignment. (For interpretation of the references to color in this figure legend, the reader is referred to the web version of this article.)

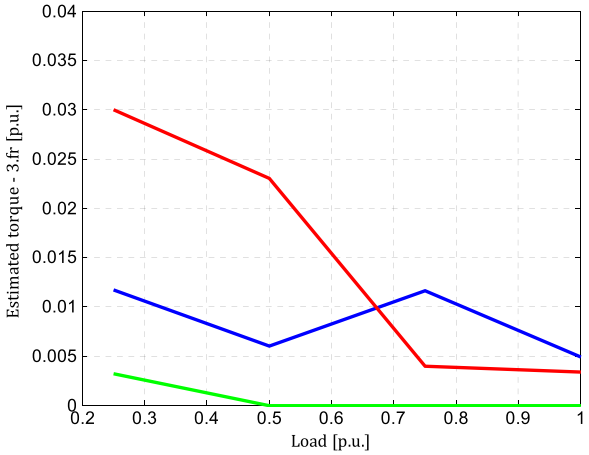

Fig. 11. Components at three times the rotation frequency. Values in p.u. Green: Alignment, Blue: 0.75 mm Radial Misalignment, Red: 1.5 mm Radial Misalignment. (For interpretation of the references to color in this figure legend, the reader is referred to the web version of this article.)

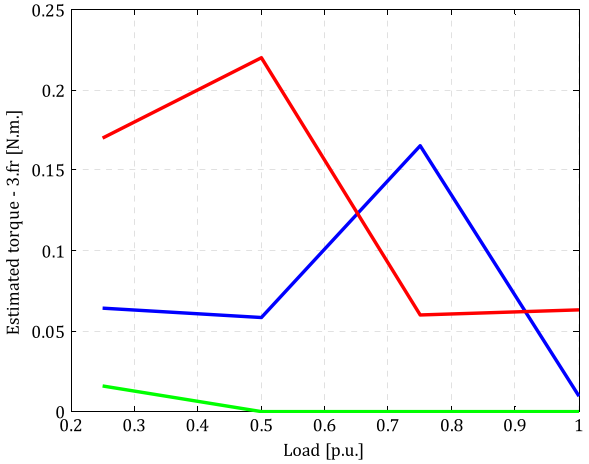

Fig. 12. Components at three times the rotation frequency. Values in N.m. Green: Alignment, Blue: 0.75 mm Radial Misalignment, Red: 1.5 mm Radial Misalignment. (For interpretation of the references to color in this figure legend, the reader is referred to the web version of this article.)

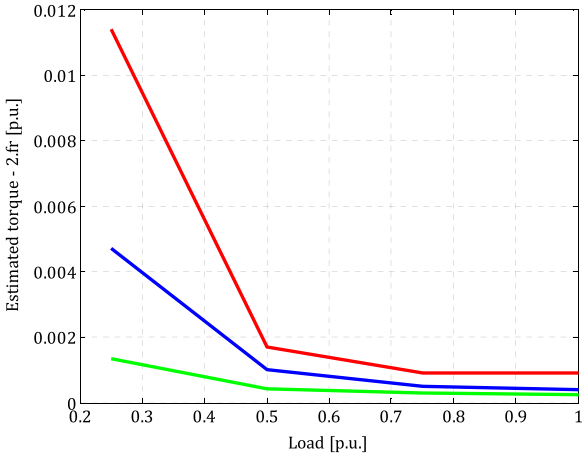

Fig. 13. Components at twice the rotation frequency. Values in p.u. Jaw Coupling. Green: Alignment, Blue: 0.5° Angular Misalignment, Red: 1° Angular Misalignment. (For interpretation of the references to color in this figure legend, the reader is referred to the web version of this article.)

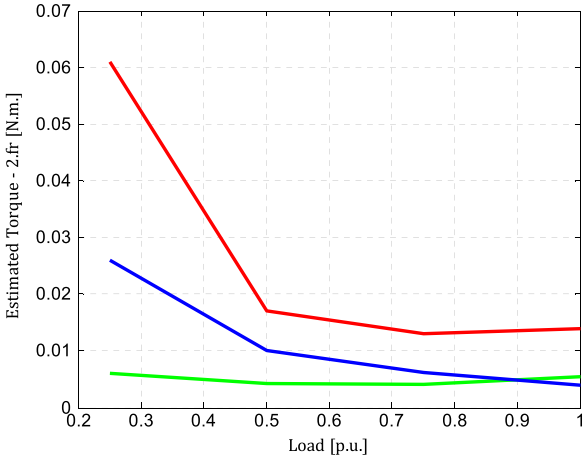

Fig. 14. Components at twice the rotation frequency. Values in N.m. Green: Alignment, Blue: 0.5° Angular Misalignment, Red: 1° Angular Misalignment. (For interpretation of the references to color in this figure legend, the reader is referred to the web version of this article.)

Table 1
Torque at *2fr* for 1°angular misalignment. Values expressed in % of the mean T.

Load (%)	Rubber Tire-type Coupling	Jaw Coupling	Gear Coupling	Metal Ribbon Coupling
25	0.22	1.13	0.67	0.51
50	0.16	0.17	0.55	0.15
75	0.09	0.14	0.45	0.09
100	0.05	0.07	0.29	0.07

same experiments carried out using the Jaw Coupling are repeated but using the other couplings shown in Fig. 2. Tables 1 and 2 display the values of the estimated torque components for 1° angular misalignment (Table 1) and 1.5 mm radial misalignment (Table 2), for each four couplings under study.

Similarly, Tables 3 and 4, present the results obtained for the stator currents (MCSA). In this case, the values presented in the tables correspond to the RMS obtained from both sidebands components.

The results obtained using the Jaw Coupling and the other couplings show similar tendency. That is, they show a decrease in the indicators as the motor load increases. In addition, it becomes clear that the obtained values, as for the estimated torque as for the stator current, are significantly different for the different couplings. In fact, for identical misalignment and load conditions, the results obtained for the different couplings show variations as for angular as for radial misalignment.

Figs. 15 and 16 show the results for the estimated torque and stator current for angular misalignment. Regarding both variables, it can be observed an important difference between the indicators associated to the Gear Coupling and those of

Table 2
Torque at *2fr* for 1.5 mm radial misalignment. Values expressed in % of the mean T.

Load (%)	Rubber Tire-type Coupling	Jaw Coupling	Gear Coupling	Metal Ribbon Coupling
25	0.24	13	2.6	4.1
50	0.14	10	3.7	2.8
75	0.06	4.1	0.66	2.7
100	0.07	2.1	0.13	1.6

Table 3
Stator current (RMS) for 1°angular misalignment – Values expressed in % of the fundamental component.

Load (%)	Rubber Tire-type Coupling	Jaw Coupling	Gear Coupling	Metal Ribbon Coupling
25	0.14	0.15	0.31	0.18
50	0.09	0.11	0.34	0.11
75	0.06	0.09	0.30	0.06
100	0.04	0.06	0.25	0.05

Table 4
Stator current (RMS) for 1.5 mm radial misalignment – Values expressed in % of the fundamental component.

Load (%)	Rubber Tire-type Coupling	Jaw Coupling	Gear Coupling	Metal Ribbon Coupling
25	0.14	5.7	1.1	2.7
50	0.07	7.3	2.9	1.5
75	0.05	3	0.48	2.2
100	0.04	2	0.13	1.9

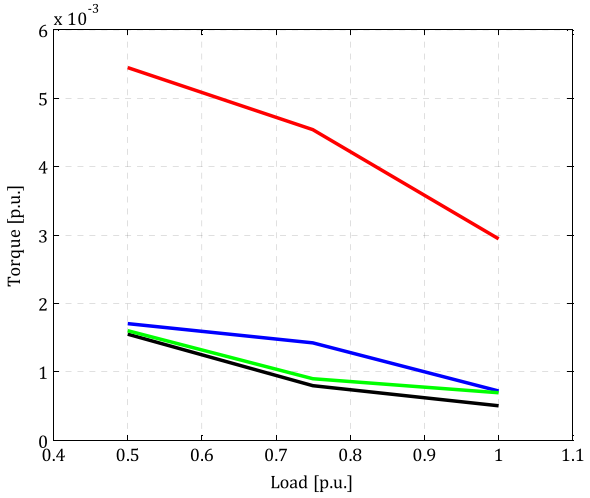

Fig. 15. Estimated Torque vs. percentage of load at angular misalignment of 1°. Red: Gear Coupling. Blue: Jaw Coupling. Green: Metal Ribbon Coupling. Black: Rubber Tire-type Coupling. (For interpretation of the references to color in this figure legend, the reader is referred to the web version of this article.)

the other couplings. The Gear Coupling shows a really low tolerance to angular misalignment due to the torque high-harmonic components of these couplings. As for the rest of the couplings under study, they all show similar behavior for angular misalignment.

Fig. 17 and 18 show results for radial misalignment. In this case, significant differences for different types of coupling are observed. The jaw coupling is the one that most clearly reflect misalignment on the fault indicators, which means low tolerance to radial misalignment. On the other hand, the Rubber Tire-type Coupling shows low fault indicators, which indicates high tolerance to radial misalignment.

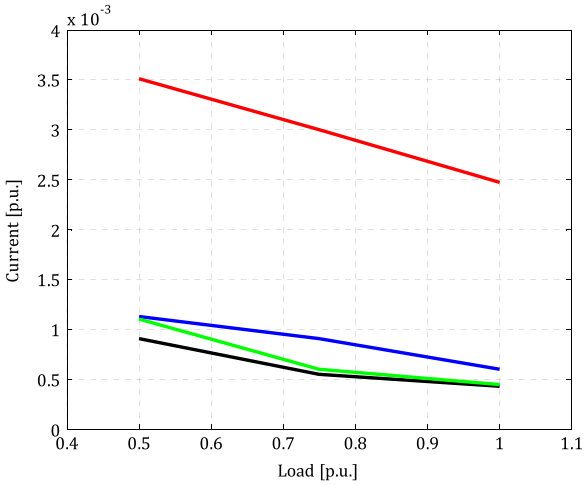

Fig. 16. Current components, $f \pm fr$ (rms) vs. percentage of load at angular misalignment of 1°. Red: Gear Coupling. Blue: Jaw Coupling. Green: Metal Ribbon Coupling. Black: Rubber Tire-type Coupling. (For interpretation of the references to color in this figure legend, the reader is referred to the web version of this article.)

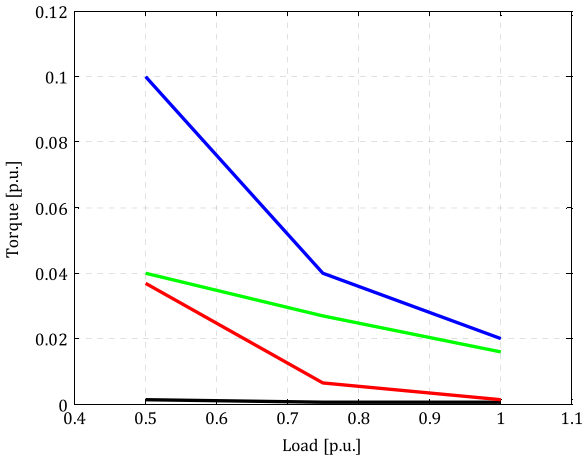

Fig. 17. Estimated Torque vs. percentage of load at radial misalignment of 1°. Red: Gear Coupling. Blue: Jaw Coupling. Green: Metal Ribbon Coupling. Black: Rubber Tire-type Coupling. (For interpretation of the references to color in this figure legend, the reader is referred to the web version of this article.)

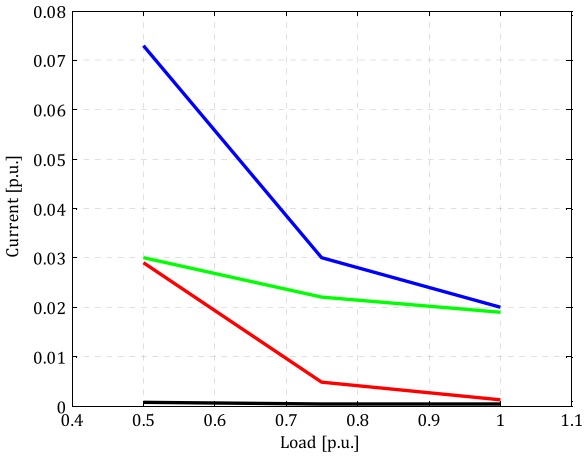

Fig. 18. Current components, $f \pm fr$ (rms) vs. percentage of load at radial misalignment of 1°. Red: Gear Coupling. Blue: Jaw Coupling. Green: Metal Ribbon Coupling. Black: Rubber Tire-type Coupling. (For interpretation of the references to color in this figure legend, the reader is referred to the web version of this article.)

5. Conclusions

From the experimental results presented in the previous section, it is concluded that both, the frequency components of the stator current (MCSA) and the estimated electrical torque (TLSA), allow identifying radial and angular misalignment when coupling induction motors and loads through flexible couplings.

Such a characteristic can be demonstrated for angular and radial misalignment and for small levels of misalignment, i.e., for incipient faults. The components of the estimated torque at *2fr* and *3fr* frequencies are suitable for detecting misalignment. The latter, however, is heavily dependent on the motor load conditions and its amplitude does not maintain, in all the cases studied, a proportional relationship with the fault levels. Therefore, it is considered a more suitable fault indicator than that of the component at *2fr* frequency.

Fault indicators, as for the MCSA as for the TLSA, show high dependence on the characteristic of the used coupling. This makes it difficult to associate fault indicators with a certain degree of misalignment, without considering the specific features of the coupling. Moreover, it is important to note that the coupling to more easily detect angular misalignment is the one with the lowest tolerance of angular misalignment (Gear Coupling), according to its manufacturer. Similarly, the lower radial misalignment tolerance given by the coupling manufacturer (Jaw Coupling) is more susceptible to radial misalignment detection. While it is not possible to draw definitive conclusions on this point, the relationship between the permissible misalignment of a coupling, given by its manufacturer, and the amplitude of fault indicators will be a subject of future studies.

Finally, the experimental study presented allows to state that the sensitivity of fault indicators strongly depends on the coupling features. Hence, in the case of automatic on-line fault detection algorithms, as the one proposed by [17], the thresholds above which alarm signals appear should be set depending on the type of coupling.

Acknowledgments

This research is supported by the ANPCYT, CONICET, Universidad Nacional del Centro de la Provincia de Buenos Aires and Universidad Nacional de Rio Cuarto (Argentina).

References

[1] H. Henao, G.A. Capolino, M. Fernandez-Cabanas, F. Filippetti, C. Bruzzese, E. Strangas, R. Pusca, J. Estima, M. Riera-Guasp, S. Hedayati-Kia, Trends in fault diagnosis for electrical machines: a review of diagnostic techniques, IEEE Ind. Electron. Mag. 8 (2) (2014) 31–42.
[2] M. Riera-Guasp, J.A. Antonino-Daviu, G.A. Capolino, Advances in electrical machine, power electronic, and drive condition monitoring and fault detection: state of the art, IEEE Trans. Ind. Electron. 62 (3) (2015) 1746–1759.
[3] E.H. El Bouchikhi, V. Choqueuse, M. Benbouzid, Induction machine faults detection using stator current parametric spectral estimation, Mech. Syst. Signal Process. 52–53 (2015) 447–464.
[4] S. Bindu, V. Thomas, Diagnoses of internal faults of three phase squirrel cage induction motor – a review, in: Proceedings of the International Conference on Advances in Energy Conversion Technologies – Intelligent Energy Management: Technologies and Challenges, ICAECT 2014, Manipal, 2014, pp. 48–54.
[5] Jee-Hoon Jung, Lee Jong-Jae, Bong-Hwan Kwon, Online Diagnosis of Induction Motors Using MCSA, IEEE Trans. Ind. Electron. 53 (6) (2006) 1842–1852.
[6] G. Acosta, C. Verucchi, E. Celso, A current monitoring system for diagnosing electrical failures in induction motors, Mech. Syst. Signal Process. 20 (4) (2006) 953–965.
[7] J. Estima, N. Freire, A. Cardoso. Recent advances in fault diagnosis by Park's vector approach, in: Proceedings of IEEE Workshop on Electrical Machines Design, Control and Diagnosis, WEMDCD 2013, París, 2013, pp. 279–288.
[8] M. Stopa, B. de Jesus Cardoso Filho, B., Load torque signature analysis: an alternative to MCSA to detect faults in motor driven loads, in: IEEE Energy Conversion Congress and Exposition (ECCE), Raleigh, NC, USA, 2012, pp. 4029–4036.
[9] S. Kia. H. Henao, G.A. Capolino. Torsional vibration assessment in railway traction system mechanical transmission, in: IEEE International Symposium on Diagnostics for Electric Machines, Power Electronics and Drives, 2009. SDEMPED 2009, Cargèse, 2009, pp. 1–8.
[10] S. Kia, H. Henao, G.A. Capolino, A comparative study of acoustic, vibration and stator current signatures for gear tooth fault diagnosis, in: Proceedings of the XXth International Conference on Electrical Machines (ICEM), 2012, Marseille, 2012, pp. 1514–1519.
[11] S. Rajagopalan, T.G. Habetler, R.G. Harley, T. Sebastian, B. Lequense, Current/voltage-based detection of fault in gears coupled to electric motors, IEEE Trans. Ind. Appl. 42 (6) (2006) 1412–1420.
[13] W. Thomson, M. Fenger, Current signature analysis to detect induction motor faults, IEEE Ind. Appl. Mag. 7-4 (2001) 26–34.
[14] M. Stopa, B. Cardoso Filho, C.B. Martinez, Incipient Detection of Cavitation Phenomenon in Centrifugal Pumps, IEEE Trans. Ind. Appl. 50 (1) (2014) 120–126.
[15] J.M. Bossio, G. Bossio, C. De Angelo, Angular Misalignment in Induction Motors with Flexible Coupling, in: Proceedings of IEEE Industrial Electronics Conference, 2009. IECON'09, Porto, 2009, pp. 1033–1038.
[16] R. Obaid, T. Hableter, Effect of Load on Detecting Mechanical Faults in Small Induction Motors, in: Proceedings of Symposium on Diagnostics for Electric Machines, Power Electronics and Drives, SDEMPED 2003, Atlanta, 2003, pp. 307–311.
[17] R. Obaid, T. Hableter, T., Current-Based Algorithm for Mechanical Fault Detection in Induction Motors with Arbitrary Load Conditions, in: Conference Record of the 38th IAS Annual Meeting, Salt Lake, 2003, pp: 1347-1351.
[18] J. Piotrowski, Shaft Alignment Handbook, Third Edition, CRC Press, Ohío, 2006.
[19] C. Salomón, W. Santana, L. da Silva, E. Bonaldi, L. de Oliveira, J. da Silva, G. Lambert-Torres, A. Donadon, A stator flux synthesis approach for torque estimation of induction motors using a modified stator resistance considering the losses effect, in: Proceedings of IEEE International Electric Machines & Drives Conference (IEMDC), Chicago, 2013, pp. 1369–1375.